Journal of the Korean Physical Society, Vol. 47, No. 1, July 2005, pp. 142∼147

Indium-Oxide Thin Films Deposited by Using an Oxygen-Ion-Beam-Assisted Deposition Technique for Top-Emitting Organic Light-Emitting Diodes

J. T. Lim,* N. G. Cho, C. H. Jeong, J. H. Lee, J. H. Lim and G. Y. Yeom

Department of Materials Engineering, SungKyunKwan University, Suwon 440-746

(Received 30 December 2004, in final form 28 April 2005)

To fabricate a top-emitting organic light-emitting diode (TEOLED) with a high aperture ratio and high resolution, we deposited an n-type indium oxide (IO) as a transparent conducting electrode, by using oxygen-ion-beam-assisted deposition (IBAD), on a device of glass/ITO/NPB (60 nm)/Alq_3 (60 nm)/LiF (1 nm)/Al (2 nm)/Ag (20 nm), and we investigated its characteristics. To minimize the damage to the organic layers and the oxidation of the Ag layer during the oxygen IBAD, we required a two-step processing of IBAD composed of argon IBAD followed by oxygen IBAD. By the two-step processing of the IO thin film deposition using IBAD, TEOLED devices having emission on both sides could be formed successfully with an external quantum efficiency of 0.47 % and a luminous efficiency of 0.22 lm/W at a luminance of about 100 Cd/m^2. With this device, a maximum luminance of 12,500 Cd/m^2 was obtained at the glass surface of the device. Even though the overall quantum efficiency of this device was very low, we believe that it can be improved by optimizing oxygen-ion-beam processing used to fabricate the IO thin films and by optimizing the thickness of the semitransparent conducting protecting layer to reduce ion-beam-induced damage.

PACS numbers: 81.15.J, 72.80.L
Keywords: IBAD, Organic semiconductors, Top emission, TEOLED, IO, Protective buffer layer

I. INTRODUCTION

Organic light-emitting diodes (OLEDs) are the most promising next-generation large-area flat-panel displays since Tang and Van Slyke reported an efficient double-layered OLED utilizing tris(8-quinolinolato-N^1,O^3) aluminum (III) (Alq_3) [1,2] and have been widely studied since the display panel fabricated by a Japanese OLED manufacturer, Pioneer, was put on to the market in 1998 [3,4]. Also, many kinds of transparent conducting oxides (TCOs) films have been widely used as the conductors for numerous opto-electronic applications. For the application to top-emitting organic light-emitting diodes (TEOLEDs), the n-type single component and the multi-component TCOs [5–7] consisting of In_2O_3 (IO), SnO_2, and ZnO are actively being studied to obtain a low resistivity, a high transmittance for higher response rate, a low power consumption, a high aperture ratio, an excellent color purity, and a semi-passivation effect. They are also being studied for possible applications to color filters and color-changing media. A successful application of TCOs to OLEDs for TEOLEDs can improve the display performances of conventional active-matrix OLEDs (AMOLEDs). Especially, when TEOLEDs are used for active-matrix addressing, device performances, such as power consumption and lifetime, can be drastically improved because the emitting area depends on neither the design of the pixel circuits nor the number of thin-film transistors located below the OLED [8]. In fact, an active matrix TMOLED with a higher aperture ratio and a higher resolution of XVGA (1024 × 768) is a prerequisite for a panel size above 5-inch diagonal; therefore, the study on TCOs applied to TEOLEDs is very important for achieving large-sized and high-resolution OLED devices.

Intensive studies on conventional bottom-emitting OLEDs have been well documented. However, there is very limited information on the fabrication of TEOLED devices. In general, the use of rf-sputtered ITO thin films as top transparent capping-electrodes together with thin transparent or semi-transparent protective buffer layers, such as MgAg [9, 10], copper phthalocyanine [11], Li/CuPc [12], Li/2,9-dimethyl-4,7-diphenyl-1,10-phenanthroline [13], Ca and/or LiF/Al [14], 3,4,9,10-perlyenetetracarboxylic dianhydride [11], metal acetylacetonate complexes [15], and pentacene [16], have been reported. However, the damage to the underlying organic layer induced by oxygen ions during sputter deposition is one of the major problems in the formation of a TCO on a device for a TEOLED.

Various methods can be used to deposit TCOs on OLED devices, and one of the methods is to use oxygen-ion-beam-assisted deposition (IBAD). An oxygen IBAD

*E-mail: lapbbi@skku.edu; Fax: +82-2-299-6565

system includes an ICP-type ion gun as the source of oxygen ions and atomic oxygen radicals and an electron-beam evaporator as the TCO source. In general, during the processing of TCO thin films, by rf or dc sputtering, on the organic layers of OLED devices, physical damage and oxidation of the organic layers is inevitable due to the energy of the oxygen-ion radicals in the plasma. In the case of IBAD, if an IBAD system with the ion gun facing the substrate holder at an angle of 30 $\sim$ 40° is used, the physical damage to the substrate can be significantly decreased while supplying enough oxygen to the substrate to form conductive and transparent TCOs at room temperature. However, due to the oxygen ion beam, the semitransparent ohmic contact metal layer of the TEOLED can be oxidized. If oxidation of the ohmic metal layer of the OLED is to be prevented, before using the oxygen ion beam, an argon ion beam can be used during the deposition of the TCO to the TEOLED by using argon instead of oxygen for the ion gun of the IBAD system.

In this paper, using the above two-step TCO deposition method, we deposited IO as the TCO electrode on a semitransparent metal ohmic contact of a TEOLED device, and we investigated its effect on the damage to the device by measuring the current density - voltage - luminance curves of the fabricated TEOLED devices. The IO deposition condition was also investigated in order to optimize the electrical and the optical properties of IO.

II. EXPERIMENTAL DETAILS

1. Fabrication of the Organic Light-emitting Devices Emitting on Both Sides

The devices were fabricated by vacuum evaporation of organic layers and a LiF/Al/Ag buffer layer on top of a glass substrate coated with indium tin oxide (ITO) with a sheet resistance of about 10 Ω/□. The glass substrate coated with ITO was cleaned by sonication in trichloroethylene (TCE), *iso*-propanol, acetone, and methyl alcohol and was rinsed in deionized water. The hole-transporting layer (HTL), 4,4'-bis[N-(1-napthyl)-N-phenyl-amino]-biphenyl (α-NPD) having a thickness of 60 nm, was deposited on ITO by thermal evaporation under a base pressure of 7×10^{-7} Torr. On top of a-NPD, tris(8-hydroxyquinolinonato)aluminium (III) (Alq_3) was deposited as a green emissive and electron-transporting layer with a thickness of 60 nm. Next, 1-nm-thick lithium fluoride (LiF) was deposited as an electron-injecting layer. Then, 2-nm-thick aluminum (Al) metal and 20-nm-thick silver (Ag) metal were continuously deposited as the buffer layer to protect the organic layers and as the semitransparent conducting metal layer. The deposition rates and the thicknesses of the deposited layers were monitored by using a thickness/rate controller. The deposition rates for the organic layers, the LiF layer, and the Al/Ag cathode layers were 0.5 $\sim$ 2.0, 0.1 $\sim$ 0.2, and 0.5 $\sim$ 10.0 Å/sec, respectively, and the emissive active area of the device was 2 mm × 2 mm.

Current-voltage characteristics were measured with a Keithley 236 source-measure unit. Light outputs from the emissions of the devices emitting on both sides were determined by using a Keithley 485 picoammeter to measure the photocurrent induced on silicon photodiodes. The external quantum efficiency (QE), the ratio of emitted photons to injected charges, was calculated from the luminous output measured by using a calibrated Si photodiode.

2. Deposition of IO Thin Films on the OLED Emitting on Both Sides by Using an IBAD System

The IO deposition was conducted using an oxygen IBAD system. The ion gun of the IBAD system was facing the substrate holder at an angle of 30 $\sim$ 40° to the surface normal of the substrate to decrease the physical damage to the substrate. The schematic diagram of the deposition system is shown in Fig. 1. The IBAD system consisted of the electron beam evaporator for the evaporation of IO and an internally mounted inductively coupled ion gun for the supply of argon or oxygen ions to the substrate. The ion gun was driven by an rf inductively coupled plasma of 13.56 MHz. Also, two grids were used to efficiently extract and accelerate the generated ions and were insulated by ceramics located between them.

The IO thin film deposition was carried out in two steps at room temperature, that is, first, by using argon-ion-assisted deposition of IO and, next, by using oxygen-ion-assisted deposition of IO during the evaporation of IO. For the argon-ion-assisted deposition of IO, the Ar ion gun was operated for 200 seconds at an rf power of

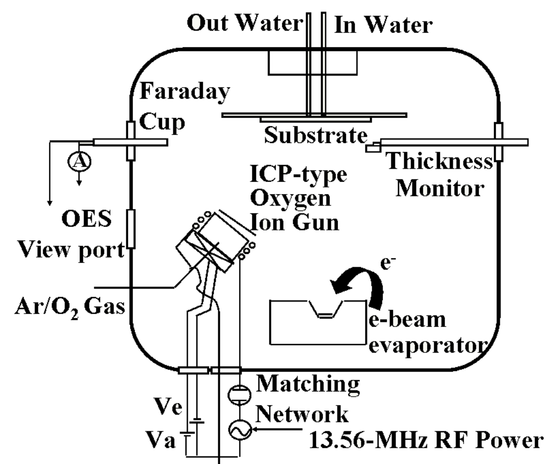

Fig. 1. Schematic diagram of the IBAD system used in this study.

250 W, a voltage of +600 V to the acceleration grid, and a voltage of 0 V to the extraction grid while flowing the argon gas at 4 sccm to the ion gun. In the case of oxygen-ion-assisted evaporation, the ion gun was operated at rf powers of 200 ~ 400 W, voltages of +200 ~ +350 V to the acceleration grid, and a voltage of 0 V to the extraction grid while flowing the oxygen gas at between 3 and 7 sccm to the ion gun. The deposition rate of the IO thin film was varied from 0.02 to 0.05 nm/sec. The source for the electron beam evaporation was a pellet of IO with 99.99 % purity (PURE TECH Co. Ltd.).

Optical emission spectroscopy (OES, SC Tech. Inc. PCM-420) was used to investigate the plasma species during the operation of the ion source as the oxygen-ion source. The resistivity and the transmittances of the deposited IO thin films were measured using a four-point probe (CMT-SERIES CHANG MIN Co. Ltd.) and a UV spectrophotometer (UV S-2100 SCINCO Inc.), respectively.

III. RESULTS AND DISCUSSION

The device structure of the transparent conducting OLED emitting on both sides is glass/ITO/α-NPD (60 nm)/Alq_3 (60 nm)/LiF (1 nm)/Al (2 nm)/Ag (20 nm)/In_2O_3 (100 nm). Using a thermal evaporation OLED deposition system located next to the IBAD, we deposited sequentially without breaking vacuum, stacked organic layers on the ITO patterned glass and a shadow-masked protective conducting buffer layers composed of a 1-nm-thickness LiF layer, a 2-nm-thickness Al layer, and a 20-nm-thickness Ag layer. Among these layers, the buffer layer of the LiF (1 nm)/Al (2 nm)/Ag (20 nm) system plays important roles, such as protecting the organic layers from oxygen-ion bombardment, electric charging, heat, light, *etc.* from the ion gun and forming a semi-transparent conducting layer. Efficient electron injection from a cathode into the Alq_3 layer can be obtained when the work function of a cathode is similar to an electron affinity of the Alq_3 layer. Also, efficient injection closely depends on the work function of LiF/Al neighboring with the Alq_3 layer which is two-component electrode of the cathode scheme consisting of LiF/Al/Ag/IO. Hung *et al.* proved that a LiF/Al bilayer with an Al layer as thin as 0.1 nm is sufficient to form an effective electron-injecting contact to the Alq_3 surface by comparing turn-on voltages and luminous efficiencies as functions of the LiF thickness on a glass/ITO/NPB/Alq_3/LiF/Al/Ag device [17]. The 2-nm-thick Al layer used in this study should exhibit an efficient electron-injecting ability and electron hopping from the LiF/Al layer to the Alq_3 layer in the view of device performance. If the Al/Ag buffer layers are made thicker, more conductive and protective properties can be obtained, but the light output from the top side of the device will be decreased by the low transmittance property of buffer layers.

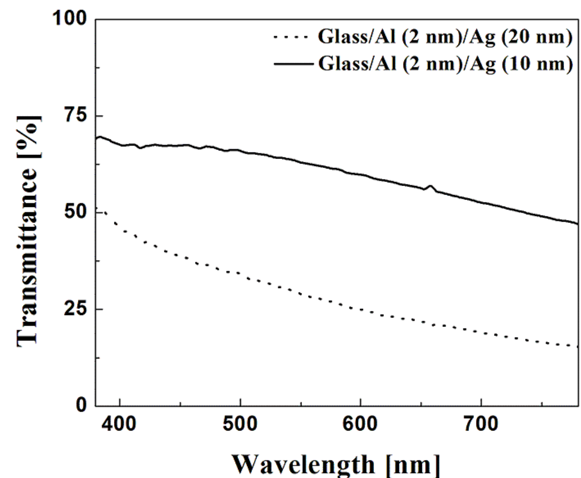

Fig. 2. Optical transmittances of glass/Al (2 nm)/Ag (x nm): x = 10 (dotted line) or 20 (solid line).

Fig. 2 shows the optical transmittance of the Al/Ag layers. Buffer layers with Al (2 nm)/Ag (20 nm) and Al (2 nm)/Ag (10 nm) structures deposited on a glass substrate exhibit transmittances of 31 and 64 % at a wavelength of 530 nm, respectively. In this experiment, to minimize damage to the organic layers and the Ag layer caused by the oxygen ions, we chose the Al (2 nm)/Ag (20 nm) buffer layer to follow the deposition of an IO layer.

In the IBAD, one of the most important factors affecting the properties of the deposited films is known to be the relative ratio between the ion-beam flux and evaporated vapor flux. However, in the case of a reactive ion beam, not only the ion beam flux to the substrate but also reactive radicals generated in the ion gun can affect the properties of the deposited film. To investigate the effect of reactive radicals on the film properties, we measured the characteristics of the plasma inside the ion gun by using OES.

Fig. 3(a) shows the optical emission peaks of oxygen ions and atoms oxygen radical measured by using OES at an oxygen flow rate of 5 sccm. The other deposition conditions, such as the rf power to ion gun, the bias voltage to the extraction grid, the voltage to the acceleration grid, the distance between the ion gun and the substrate holder, and the deposition rate of indium oxide source, were maintained at 250 W, 0 V, 250 V, 65 cm, and 0.05 nm/sec, respectively. Optical emission peaks related to positive molecular oxygen ions (O_2^+) and atomic oxygen radicals (O^*) were identified. Among these emission peaks, the O_2^+ peak at 558 nm and the O^* peak at 614 nm were selected for further investigations.

Fig. 3(b) shows the variation of the peak intensities of O_2^+ and O^* as functions of the oxygen gas flow rate to the ion gun while the other deposition conditions were kept the same as those in Fig. 3(a). As Fig. 3(b) shows, the O_2^+ and the O^* peak intensities were, respectively, increased by increasing the oxygen gas flow rate. Bae *et al.*

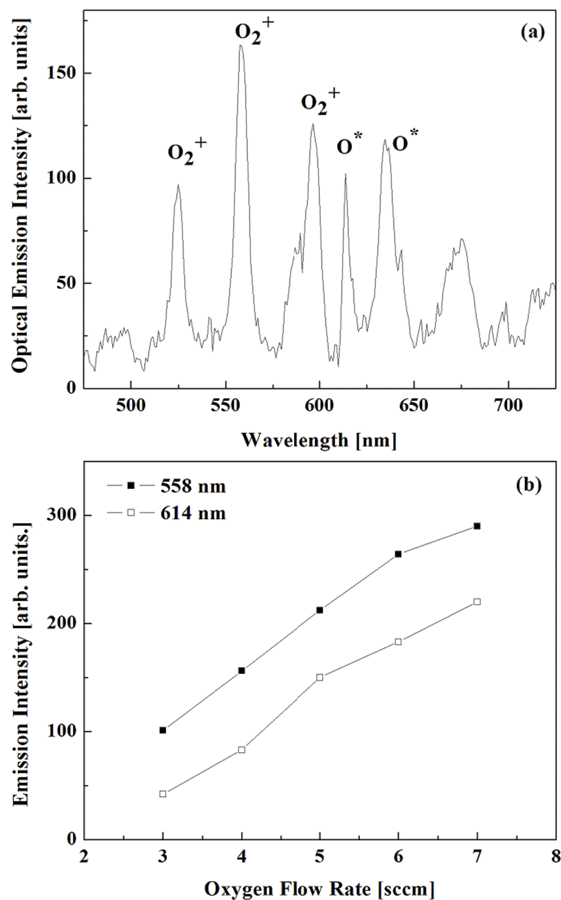

Fig. 3. (a) Optical emission spectrum of the oxygen plasma measured by using OES at an oxygen flow rate of 5 sccm, an rf power of 250 W, a Va of 250 V, and a Ve of 0 V. (b) Optical emission intensities of O_2^+ at the wavelength of 558 nm and O^* at the wavelength of 614 nm as functions of the oxygen flow rate with the other conditions the same as shown in (a).

[18], by using OES and a Faraday cup, reported that the improved electrical and optical properties of ITO thin film could be related to the incorporation of low-energy oxygen radicals into the deposited ITO film rather than to the irradiation of the substrate with high-energy oxygen ions and obtained an ITO thin film with the lowest resistivity at an oxygen flow rate of 6 sccm to the ion gun. Although our experimental conditions are different from those of Bae *et al.*, our IO thin film deposited on a glass substrate exhibited the best properties with a resistivity of 6.5×10^{-4} Ω· cm and a transmittance of 97 % at an oxygen flow rate of 5 sccm.

Meanwhile, as the rf power to the ion gun was increased, the electrical resistivity at rf powers above and below 250 W increased greatly while the extraction voltage, the acceleration voltage, the distance between ion gun and the substrate holder, and the IO deposition rate were 0 V, 250 V, 65 cm, and 0.05 nm/sec, respectively, indicating the optimal oxygen incorporation occurred at an rf power of 250 W.

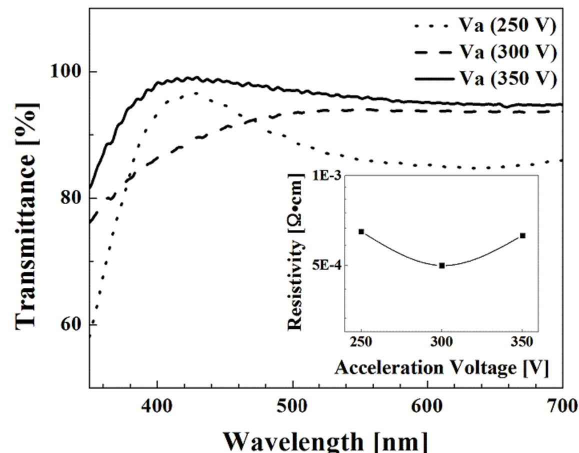

Fig. 4. Transmittances of deposited IO thin films as a function of the acceleration voltage to the ion gun at a rf power of 250 W, an extraction voltage of 0 V, an oxygen flow rate of 5 sccm, and a deposition rate of 0.05 nm/sec. The inset shows the resistivity of IO thin films deposited as a function of the acceleration voltage (solid line: 350 V; dashed line: 300 V; and dotted line: 250 V).

The final optimization of the IO deposition conditions of the oxygen-ion-assisted evaporation was conducted by varying the acceleration voltage of the oxygen ion gun from 250 to 350 V while keeping the other conditions, such as the evaporation rate (0.05 nm/sec) of IO, the rf power (250 W), the extraction voltage (0 V) to the oxygen ion gun, the oxygen flow rate (5 sccm) to the ion gun, and the distance (65 cm) between the substrate holder and ion gun, constant.

Fig. 4 and the inset of Fig. 4 show the transmittance and the resistivity of the IO deposited on the glass substrate as functions of the acceleration voltage, respectively. As the figure shows, by applying 300 V to the acceleration grid, we were able to obtain an IO thin film with the lowest resistivity of 5×10^{-4} Ω·cm and an excellent transmittance of 94 % at a wavelength of 530 nm. However, when this IO film of about 100 nm was deposited on the Al (2 nm)/Ag (20 nm) layer of the OLED device, due to the poor transmittance of the LiF/Al/Ag/IO deposited on the OLED before the IO film, the top emission of TEOLED device showed a light output loss of about 70 %.

Also, during the experimental, the Ag layer was found to be easily oxidized by the oxygen ions of IBAD system. To prevent the oxidation of the protective buffer layer of Al (2 nm)/Ag (20 nm) by the oxygen ions and the radical atoms of ion gun, we carried out the deposition of the IO thin film in two steps. First, by flowing 4 sccm of Ar to the ion gun instead of oxygen gas, we deposited a nominally 10-nm-thick IO buffer layer. The deposition conditions, rf power (250 W), acceleration voltage (+600 V), extraction voltage (0 V), and the IO deposition rate (0.02 nm/sec) were kept constant. With an acceleration voltage of +600 V and a low IO evaporation rate of 0.02

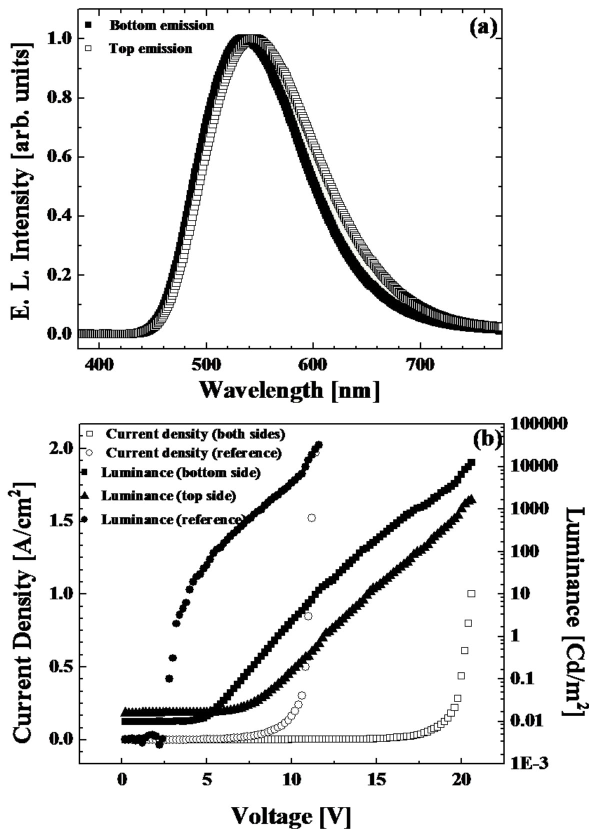

Fig. 5. (a) EL spectra of bottom (closed squares) and top-emission (open squares) from the device composed of glass/ITO/α-NPD (60 nm)/Alq_3 (60 nm)/LiF (1 nm)/Al (2 nm)/Ag (100 nm)/In_2O_3 (100 nm) device emitting on both sides at a current density of 5.43 mA/cm^2 and a luminance of about 100 Cd/m^2. (b) Current density vs. voltage (open symbols) and luminance vs. voltage (closed symbols) characteristics of the device emitting on both sides composed of glass/ITO/α-NPD (60 nm)/Alq_3 (60 nm)/LiF (1 nm)/Al (2 nm)/Ag (20 nm)/In_2O_3 (100 nm) (square symbols for top emission and triangular symbols for bottom emission) and of the reference device composed of glass/ITO/α-NPD (60 nm)/Alq_3 (60 nm)/LiF (1 nm)/Al (100 nm) (circular symbols for bottom emission).

nm/sec, the Al (2 nm)/Ag (20 nm)/ In_2O_3 (10 nm) layer showed a sheet resistance of about 5 $\Omega/\square$ with about a 25 % transmittance. Second, by using the optimized IO conditions, as shown in the inset of Fig. 4, we deposited a 90-nm-thick indium oxide. Using this two-step deposition of IO thin film, we could suppress oxidation of the Ag surface. The total sheet resistance of the Al (2 nm)/Ag (20 nm)/ In_2O_3 (100 nm) capping electrode deposited on the OLED device emitting on both sides of the ITO/a-NPD/Alq_3/LiF/Al/Ag/In_2O_3 structure was 7.5 $\Omega/\square$.

Fig. 5(a) shows the EL spectra of the OLED devices emitting green on both sides of the IO thin film deposited using the above two-step IBAD method. The EL spectra were measured at a luminance of about 100 Cd/m^2. The maximum EL peaks from the top and the bottom emissions of the device were 543 and 536 nm, respectively. The differences in the maximum wavelengths of the EL peaks from the top and the bottom of the device could be attributed to optical properties, such as the wide-angle and multiple-beam interference growing from the microcavity structure reported by Riel *et al.* [19]. This interference effect was caused by the difference in the reflectivity between the top electrode of the LiF/Al/Ag/In_2O_3 surface and the bottom ITO electrode. The emissions irradiated from both the IO and the glass surfaces show the CIE (Commission Internationale de L'Eclairege) chromaticity coordinates of (0.386, 0.534) and (0.355, 0.540) for the bottom and the top emission, respectively. These CIE coordinates are relatively apart from that of pure green, possibly due to reflections of the emitted light from various interfaces.

Fig. 5(b) shows the current-voltage-luminescence characteristics of a device composed of glass/ITO/α-NPD (60 nm)/Alq_3 (60 nm)/LiF (1 nm)/Al (2 nm)/Ag (20 nm)/In_2O_3 (100 nm), which was emitting on both sides of the glass and of a conventional device composed of glass/ITO/α-NPD (60 nm)/Alq_3 (60 nm)/LiF (1 nm)/Al (100 nm), which was emitting on the bottom of the glass as a reference of optical output. The onset voltage of the device emitting on both sides was about 7 V at a luminance of 0.1 Cd/m^2. The bottom emission of the OLED device emitting on both sides showed an external quantum efficiency of about 0.47 % and a luminous efficiency of 0.22 lm/W at a luminance of about 100 Cd/m^2 (for a bias voltage of 14 V and a current density of 4.5 mA/cm^2). The maximum luminance of the top and the bottom emissions emitting from both sides of the glass were about 2,000 Cd/m^2 and 12,500 Cd/m^2, respectively, at 20.6 V and 1.00 A/cm^2. The reference OLED device, as shown in the solid circles of Fig. 5(b) showed the maximum luminance of 32,000 Cd/m^2 at a voltage of 11.6 V and a current density of 1.97 A/cm^2. The external quantum efficiency and the luminous efficiency were 0.41 % and 0.71 lm/W at a luminance of about 100 Cd/m^2 (for a bias voltage of 5.4 V and a current density of 4.8 mA/cm^2), respectively. Therefore, the device performance obtained in this experiment was not good enough. However, we believe that it can be significantly improved by optimizing the IBAD of the IO thin film and by developing buffer layers, such as Al/Ag metal, to reduce oxygen-ion-beam-induced damage.

IV. CONCLUSIONS

A transparent conducting IO thin film was deposited on a TEOLED device composed of glass/ITO/α-NPD (60 nm)/Alq_3 (60 nm)/LiF (1 nm)/Al (2 nm)/Ag (20 nm) by using an oxygen IBAD. In this experiment, in order to reduce damage to the organic layers of the TEOLED device and to prevent oxidation of the Al/Ag semi-transparent conducting metal layer, we carried out

a two-step deposition of the IO thin film with a IBAD system. First, 10-nm-thick IO was deposited by using Ar-ion-beam-assisted evaporation; then, 90-nm-thick IO was deposited by using oxygen-ion-beam-assisted evaporation. With this two-step deposition of the IO thin film, although the indium-oxide thin film exhibited excellent physical properties, having a resistivity of 5×10^{-4} $\Omega\cdot$ cm and a transmittance of 94 %, the device showed poor light emission and a high turn-on voltage; therefore, a low quantum efficiency still remained as a problem. This was estimated to be from poor electron-injection from Ll/Al/Ag/ITO into Alq_3 due to undesirable conductance between the amorphous IO electrode and the Ag electrode. The bottom emission of the OLED device emitting on both sides, with an IO thin film fabricated by using the IBAD system, showed an external quantum efficiency of about 0.47 % and a luminous efficiency of 0.22 lm/W at a luminance of about 100 Cd/m^2. The e bottom-side mission exhibited a maximum luminance of 12,500 Cd/m^2. The ratio of the maximum luminance between the top and the bottom emissions was about 1 : 6.5.

ACKNOWLEDGMENTS

This work was supported by the Electronics and Telecommunications Research Institute (ETRI), by the National Research Laboratory Program (NRL) of the Ministry of Science & Technology, and by the Ministry of Commerce, Industry and Energy (MOCIE).

REFERENCES

[1] C. W. Tang and S. A. VanSlyke, Appl. Phys. Lett. **51**, 913 (1987).

[2] G. J. H. Burroughes, D. D. C. Bradley, A. R. Brown, R. N. Marks, K. Mackay, R. H. Friend, P. L. Burn and A. B. Homes, Nature **347**, 539 (1990).

[3] O. Prache, Displays **22**, 49 (2001).

[4] T. A. Beierlein, H. Riel and B. Ruhstaller, *Proceedings of Society for Information Displays* (Boston, 2002), p. 1260.

[5] T. Minami, MRS Bulletin **38** (2000).

[6] A. J. Freeman, K. R. Poeppelmeier, T. O. Mason, R. P. H. Chang and T. J. Marks, MRS Bulletin **45** (2000).

[7] J. S. An, S. C. Kim, S. H. Hahn, S. K. Ko and E. J. Kim, J. Korean Phys. Soc. **45**, 1629 (2004).

[8] K. T. Sasaoka, M. Sekiya, A. Yumoto, J. Yamada, T. Hirano, Y. Iwase, T. Yamada, T. Ishibashi, T. Mori, M. Asano, S. Tamura and T. Urabe, SID 01 digest, **384** (2001).

[9] G. Gu, V. Bulovic, P. E. Burrows, S. R. Forrest and M. E. Thompson, Appl. Phys. Lett. **68**, 2606 (1996).

[10] V. Bulovic, G. Gu, D. E. Burrows, M. E. Thompson and S. R. Forrest, Nature **380**, 29 (1996).

[11] G. Parthasarathy, P. E. Burrows, V. Khalfin, V. G. Kozlov and S. R. Forrest, Appl. Phys. Lett. **72**, 2138 (1998).

[12] L. S. Hung and C. W. Tang, Appl. Phys. Lett. **74**, 3209 (1999).

[13] G. Parthasarathy, C. Adachi, P. E. Burrows and S. R. Forrest, Appl. Phys. Lett. **76**, 2128 (2000).

[14] P. E. Burrows, G. Gu, S. R. Forrest, E. P. Vicenzi and T. X. Zhou, J. Appl. Phys. **87**, 3080 (2000).

[15] A. Yamamori, S. Hayashi, T. Koyama and Y. Taniguchi, Appl. Phys. Lett. **78**, 3343 (2001).

[16] T. Dobbertin, M. Kroeger, D. Meithecker, D. Schneider, D. Metzdouf, H. Neuner, E. Becker, H-H. Johannes and W. Kowalsky, Appl. Phys. Lett. **82**, 284 (2003).

[17] L. S. Hung, C. W. Tang, M. G. Mason, P. Raychadhuri and J. Madathil, Appl. Phys. Lett. **78**, 544, (2001).

[18] J. W. Bae, H. J. Kim, J. S. Kim, Y. H. Lee, N. E. Lee and G. Y. Yeom, Surf. Coat. Technol. **131**, 196 (2000).

[19] H. Riel, S. Karg, T. Beierlein and W. Reib, J. Appl. Phys. **94**, 5290 (2003).